JOURNAL OF PROPULSION AND POWER
Vol. 11, No. 1, January–February 1995

# Flow of a Fissioning Gas in an Outflow Disk Magnetohydrodynamic Generator

Gerard E. Welch,* Edward T. Dugan,† and William E. Lear Jr.‡
*University of Florida, Gainesville, Florida 32611*

**The influence of fissioning and magnetohydrodynamic (MHD) interaction on the steady, supersonic flow of a compressible, turbulent, weakly ionized, fissioning gas in an outflow disk MHD generator is investigated. The two-dimensional ($r$, $z$) MHD flow is modeled using the thin-layer Navier-Stokes equations with MHD and fission power density source terms and Maxwell's equations, simplified by the MHD approximations and by neglecting the induced magnetic field. Simple plasma physics transport property models are developed for the collision-dominated, weakly ionized plasma in which fission fragment induced ionization provides the dominant source of conduction electrons. The two-dimensional MHD solution methodology is used to characterize the effects of fission power density and variable applied magnetic induction levels on the spatial profiles of important generator variables. A comparison of the predictions of the two-dimensional MHD solver with those of a quasi-one-dimensional Euler solver with MHD and fission source terms is used to discuss the relative influence of two-dimensional effects on the generator flowfield and on performance levels. The low MHD interaction and generator performance levels predicted for the supersonic fissioning plasma suggest that the fission fragment induced ionization, by itself, is insufficient to effect the electrical conductivity levels needed for practical power generation in the outflow disk MHD generator configuration of this study.**

## Nomenclature

$\hat{\boldsymbol{A}}$ = vector of conserved fluid variables
$a$ = speed of sound
$a_1$ = constant in electron number density formula
$\boldsymbol{B}$ = $(0, 0, B_z)$, applied magnetic induction
$\hat{\boldsymbol{B}}$ = inviscid flux vector
$C_3$ = constant in three-body recombination rate coefficient
$\hat{\boldsymbol{C}}$ = inviscid flux vector
$\hat{\boldsymbol{C}}_v$ = viscous flux vector
$c_p$ = specific heat at constant pressure
$\hat{\boldsymbol{D}}$ = source term vector
$\boldsymbol{E}$ = $(E_r, E_\theta, E_z)$, electric field strength
$e$ = magnitude of electron charge
$\tilde{e}$ = specific stagnation energy
$G_f$ = energy deposited in working fluid per fission event
$\sqrt{g}$ = Jacobian of $(r, z) \leftrightarrows (\xi, \eta)$ transformation
$\tilde{h}$ = specific stagnation enthalpy
$I$ = generator load current
$J_{r,S}$ = short-circuit Hall conduction current density, $\sigma_\perp(u\beta_e + v)B_z$
$\boldsymbol{J}$ = $(J_r, J_\theta, J_z)$, conduction current density
$\boldsymbol{J}_e$ = electron conduction current density
$k_l$ = laminar thermal conductivity
$L$ = distance between anode and cathode
$M_R$ = radial Mach number, $u/a$
$M_T$ = total Mach number, $|\boldsymbol{u}|/a$
$M_w$ = fluid molecular weight
$m_e$ = electron mass
$m_H$ = "heavy" fluid atom mass
$n_e$ = electron number density
$n_0$ = fluid number density
$\tilde{P}$, $P$ = stagnation, static fluid pressure
$Pr$ = Prandtl number
$\bar{Q}_{eH}$ = effective electron-heavy momentum transfer cross section
$\dot{q}_N$ = fission power density
$\boldsymbol{q}''$ = $(q_r'', q_z'')$, heat flux
$R$ = fluid gas constant
$R_L$ = generator load resistance
$R_{MHD}$ = generator effective resistance
$Re_m$ = magnetic Reynolds number, $\mu_0\sigma_e uL$
$\boldsymbol{r}$ = $(r, \theta, z)$ cylindrical coordinates
$S$ = swirl factor, $v/u$
$S_{ff}$ = fission fragment induced electron source density
$\tilde{T}$, $T$ = stagnation, static fluid temperature
$T_e$ = electron temperature
$T_{NON}$ = nonequilibrium contribution to electron temperature
$t$ = time
$\boldsymbol{U}_e$ = electron diffusion velocity
$u_\tau$ = characteristic velocity of turbulence, $\tau_w/\rho_w$
$\boldsymbol{u}$ = $(u, v, w)$, fluid velocity
$V_L$ = generator load voltage
$w_{ff}$ = average fission fragment energy deposition per created ion-pair
$w_{ke}$ = average kinetic energy of subexcitation energy electrons
$w_r$ = average energy release per recombination event
$z^+$ = axial distance in law-of-the-wall coordinates, $zu_\tau\rho_w/\mu_w$
$\alpha_3$ = three-body electron-stabilized recombination rate coefficient
$\beta_e$ = electron Hall parameter
$\beta_f$ = atom-fraction of fissionable atoms
$\gamma$ = ratio of specific heats
$\delta$ = inelastic scatter factor
$\varepsilon_0$ = permittivity of free space
$\varepsilon$ = energy of first ionization potential
$\zeta$ = current load parameter, $J_r/J_{r,S}$

Received June 6, 1993; presented as Paper 93-3163 at the AIAA 24th Fluid Dynamics, Plasmadynamics, and Lasers Conference, Orlando, FL, July 6–9, 1993; revision received Sept. 15, 1993; accepted for publication March 31, 1994. 

*National Research Council Research Associate; currently Aerospace Engineer, U.S. Army Research Laboratory, Vehicle Propulsion Directorate, NASA Lewis Research Center, M/S 77-6, 21000 Brookpark Road, Cleveland, OH 44135. Member AIAA.

†Associate Professor of Nuclear Engineering Sciences, 202 NSC. Member AIAA.

‡Assistant Professor of Mechanical Engineering, 237 MEB. Member AIAA.

$\mu_e$ = electron mobility
$\mu_l$ = laminar viscosity
$\mu_0$ = permeability of free space
$\bar{\nu}_{eH}$ = average electron-heavy collision frequency
$\xi$ = $(\xi, \eta)$, boundary-fitted coordinates
$\rho$ = fluid mass density
$\rho^c$ = electric charge density
$\sigma_e$ = scalar electrical conductivity
$\sigma_\perp$ = Hall electrical conductivity
$\bar{\sigma}_f$ = average neutron fission cross section
$\tau_w$ = wall shear stress magnitude
$\bar{\tau}$ = shear stress tensor
$\Phi$ = neutron flux level
$\varphi$ = current density stream function
$\omega$ = relaxation factor for load current iteration

*Subscripts*
$w$ = wall value
$\infty$ = freestream value

## I. Introduction

THE magnetohydrodynamic (MHD) flow of a weakly ionized fissioning gas in an outflow disk MHD generator is studied in this work. The generator is an integral part of the moderator/reflector assembly of the conceptual space nuclear reactor power system shown in Fig. 1, so that high thermal neutron flux levels (e.g., $10^{16}$ n/cm$^2$·s) exist throughout the generator duct.[1] The 200-MW$_e$ net power system is designed to operate for approximately 1 h.[2] This short-term, high-power operation influences the choice of working fluid, the system temperatures, and neutron flux levels. The generator working fluid is a single-phase uranium tetrafluoride ($UF_4$)-He or $UF_4$-metal fluoride gas mixture containing significant atom fraction (≃5%) of the fissionable isotope $^{235}U$, so that high fission rate densities (© $10^{18}$/m$^3$·s) and fission power densities (© 10 MW$_{th}$/m$^3$) occur by design within the generator duct. The fission fragment induced ionization of the working fluid provides the dominant source of conduction electrons necessary for the electrical conductivity levels (© 1–10 S/m) required for effective MHD interaction.

The purpose of this work is to describe a theoretical model developed to analyze the effects of the fission energy deposition and MHD interaction on the steady, supersonic flow of a weakly ionized fissioning gas in the outflow disk MHD generator. No attempt is made to design the generator to optimize performance levels in the current study; rather, this work seeks to identify the effects of fission energy deposition and MHD interaction on the important generator fluid flow and electromagnetic variables. The study restricts attention to a relatively low static temperature (e.g., 1025–2100 K), unseeded, working fluid in which thermal ionization is negligible and fission fragment ionization produces the conduction electrons. The outflow disk MHD generator is first described. An overview of the fluid mechanics, electromagnetics, and fission fragment-induced plasma transport property modeling and numerical solution methodology is then provided. Example results are used to characterize the effects of fission energy deposition and MHD interaction on the spatial profiles of important generator variables. The two-dimensional computations of the present study are then compared with quasi-one-dimensional computations to both show agreement and indicate the importance of two-dimensional loss mechanisms.

## II. Generator Description

The outflow disk MHD generator is an internal flow device (see Fig. 2) in which a working fluid, containing a finite electrical conductivity, flows predominantly radially from an inlet at the center of the disk, outward between two walls (disks), through an applied axial magnetic field. The high-temperature working fluid is exhausted from an upstream plenum (e.g., furnace or reactor core), through a nozzle region, and into the disk MHD generator active volume, as shown. The flow is accelerated in the nozzle region that typically contains turning vanes that impart tangential momentum to the flow, imposing swirl ($S \equiv v/u$) on the flow to enhance generator performance levels.[3]

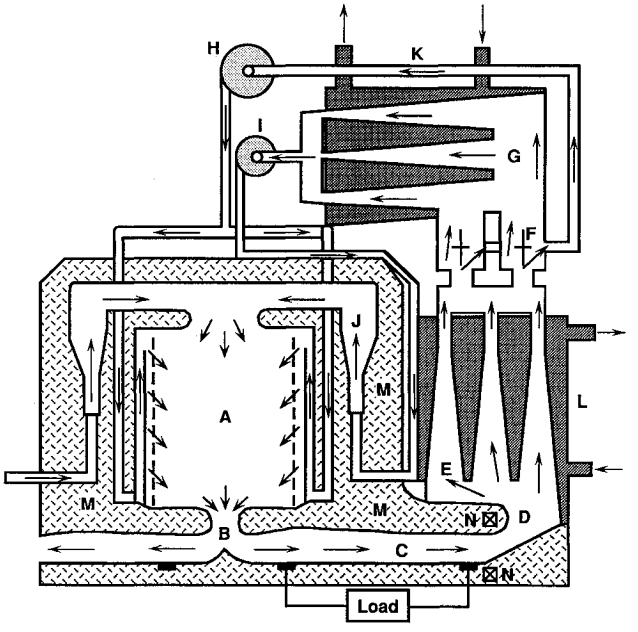


A. Gas Core Chamber
B. Supersonic Nozzle
C. Disk MHD Generator
D. Diffuser
E. Main Condenser
F. Separators
G. Secondary Condenser
H. Metal Fluoride Pump
I. $UF_4$ Pump
J. $UF_4$ Boiler
K. Secondary Radiator
L. Primary Radiator
M. BeO Moderator-Reflector
N. Magnet Windings

Fig. 1 Schematic diagram of a conceptual space nuclear reactor system using outflow disk MHD generator direct energy conversion.[16]

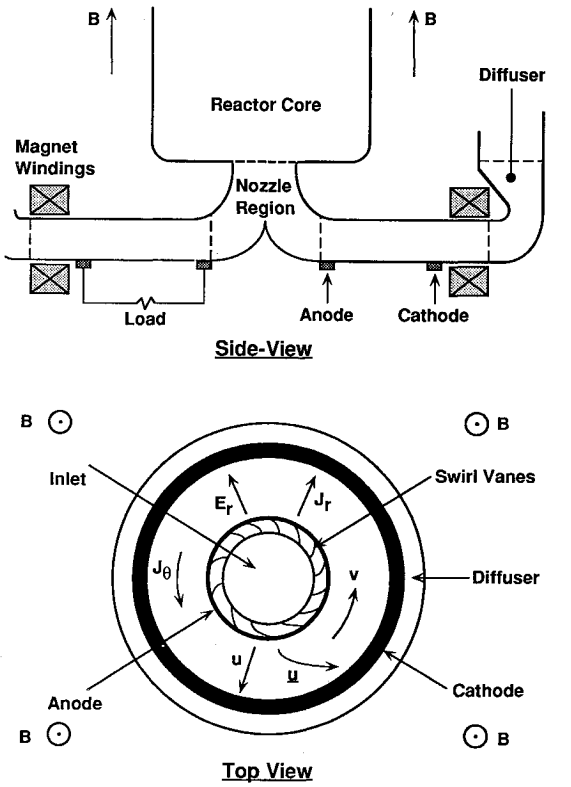


Fig. 2 Schematic diagrams of the outflow disk MHD generator.

The disk generator is a Hall device. By design, the emf-driven tangential Faraday current density component closes upon itself in short-circuit, and the Faraday field is (ideally) zero. The Hall (radial) current density arises due to the interaction of the partially ionized swirling flow with the magnetic field and by the Hall effect. The Hall effect again works on the Hall current to reduce the magnitude of the tangential Faraday current. The generator electric power density is the product of the Hall current density and the Hall electric field strength whose magnitudes are dependent in part on the load resistance that connects the anode ring, located at the generator inlet, and the downstream cathode ring. Although the inlet swirl vanes can introduce temperature and velocity "streamers" that lead to tangential asymmetries (e.g., in the plasma transport properties), the generator flow and electromagnetic fields are assumed tangentially uniform in this study. The generator analysis is restricted to the two-dimensional $(r, z)$ plane shown in the Fig. 2 side view.

The MHD generator flows considered in this study are supersonic ($M_R$ = radial Mach number = $u_r/a \geq 1$). Depending on the duct cross-sectional variation with radial position, the active generator length in which the flow remains supersonic can be restricted by the MHD interaction levels.[4] In the present work, the MHD interaction levels are low and the generator length is limited instead by the requirement that the generator active volume lie within the high neutron flux level region (e.g., $r \leq 1.3$ m) of the nuclear reactor moderator/reflector so that high fission densities are effected in the generator working fluid. The axial fission density profile within the generator closely follows the local fluid density profile because the range of the high-energy fission fragments is small ($\mathcal{O}$ 1 cm), and because there is insignificant axial neutron flux depression in the generator region.

## III. Theoretical Modeling

A brief overview of the fluid mechanics, electromagnetics, and plasma physics modeling used for predicting the behavior of the MHD generator flow is presented in this section. More thorough discussions are available elsewhere.[5,6] The equations of magnetohydrodynamics—i.e., the continuum description of fluid mechanics and electromagnetics—govern the behavior of collision-dominated plasma in continua. The "MHD approximations"[7] have been imposed in this analysis: The displacement $\partial(\varepsilon_0 \boldsymbol{E})/\partial t$ and convection $\rho^c \boldsymbol{u}$ current densities are neglected relative to the conduction current density $\boldsymbol{J}$; and the electrostatic body force $\rho^c \boldsymbol{E}$, and the convection current body force $\rho^c \boldsymbol{u} \times \boldsymbol{B}$, are neglected relative to the $\boldsymbol{J} \times \boldsymbol{B}$ body force. In addition, the induced magnetic induction $\boldsymbol{B}^i$ is negligible compared with the applied magnetic induction $\boldsymbol{B}$ at the magnetic Reynolds numbers encountered in this work ($Re_m \leq \mathcal{O}\, 10^{-2}$), and ion-slip is assumed negligible.

Tangential-symmetry ($\partial/\partial\theta = 0$) is assumed so that the analysis is restricted to the two-dimensional $(r, z)$ plane shown in the side view of Fig. 2. The tangential-symmetry is an idealization. In reality, the inlet swirl vanes can introduce wakes that lead to tangential-asymmetries, e.g., in the plasma transport properties.[8] The plasma nonuniformities are expected to degrade generator performance levels (cf. Rosa[9]); however, the electrical conductivity of the fissioning plasma is much less sensitive to static temperature variation than thermal ionization plasmas (as shown below) so that the impact of vane-induced (wakes) temperature "streamers" on performance is expected to be less severe.

The working fluid is treated as a dissociation-free, single-component, perfect gas, and the generator is analyzed in steady-state operation. Under these assumptions, the MHD equations are reduced to a set of steady-state ($\partial/\partial t = 0$) equations; however, in practice, a time-marching solution scheme is used to integrate the time-dependent form of the fluid equations asymptotically into the steady-state solution.

### A. Fluid Mechanics

The MHD flowfield is modeled using the time-averaged compressible Navier-Stokes equations with MHD ($\boldsymbol{J} \times \boldsymbol{B}$ and $\boldsymbol{J} \cdot \boldsymbol{E}$) and fission power density ($\dot{q}_N$) source terms. The governing equations are first written in cylindrical coordinates $(r, \theta, z)$,[10] and tangential-symmetry is imposed. The equations are then transformed[11-13] into the boundary-fitted coordinate system $(\xi, \eta)$, and the thin-layer approximation[14] is imposed by neglecting diffusion terms with derivatives with respect to $\xi$, the principle flow direction. Under the thin-layer approximation, the governing fluid equations can be written as

$$\frac{\partial \hat{\boldsymbol{A}}}{\partial t} + \frac{\partial \hat{\boldsymbol{B}}}{\partial \xi} + \frac{\partial \hat{\boldsymbol{C}}}{\partial \eta} = \frac{\partial \hat{\boldsymbol{C}}_\nu}{\partial \eta} + \hat{\boldsymbol{D}} \tag{1}$$

where $\hat{\boldsymbol{A}} = \sqrt{g}r(\rho, \rho u, \rho v r, \rho w, \rho \tilde{e})^T$ is the vector of conserved variables, $\hat{\boldsymbol{B}}$ and $\hat{\boldsymbol{C}}$ are the inviscid flux vectors given by

$$\hat{\boldsymbol{B}} = \sqrt{g}r \left[ \xi_r \begin{pmatrix} \rho u \\ \rho u^2 + P \\ \rho u v r \\ \rho u w \\ \rho \tilde{h} u \end{pmatrix} + \xi_z \begin{pmatrix} \rho w \\ \rho u w \\ \rho v w r \\ \rho w^2 + P \\ \rho \tilde{h} w \end{pmatrix} \right]$$

$$\hat{\boldsymbol{C}} = \sqrt{g}r \left[ \eta_r \begin{pmatrix} \rho u \\ \rho u^2 + P \\ \rho u v r \\ \rho u w \\ \rho \tilde{h} u \end{pmatrix} + \eta_z \begin{pmatrix} \rho w \\ \rho u w \\ \rho v w r \\ \rho w^2 + P \\ \rho \tilde{h} w \end{pmatrix} \right]$$

where $\hat{\boldsymbol{C}}_\nu$ is the viscous flux vector given by

$$\hat{\boldsymbol{C}}_\nu = \sqrt{g}r \left[ \eta_r \begin{pmatrix} 0 \\ \tau_{rr} \\ r\tau_{r\theta} \\ \tau_{rz} \\ (\underline{\tau} \cdot \boldsymbol{u})_r - q_r'' \end{pmatrix} + \eta_z \begin{pmatrix} 0 \\ \tau_{rz} \\ r\tau_{\theta z} \\ \tau_{zz} \\ (\underline{\tau} \cdot \boldsymbol{u})_z - q_z'' \end{pmatrix} \right]$$

and $\hat{\boldsymbol{D}}$ is the source vector given by

$$\hat{\boldsymbol{D}} = \sqrt{g}r \begin{bmatrix} 0 \\ (1/r)(\rho v^2 + P + \tau_{\theta\theta}) + J_\theta B_z \\ -rJ_r B_z \\ 0 \\ J_r E_r + J_z E_z + \dot{q}_N \end{bmatrix}$$

We have denoted fluid velocity $\boldsymbol{u} = (u, v, w)$, conduction current density $\boldsymbol{J} = (J_r, J_\theta, J_z)$, electric field strength $\boldsymbol{E} = (E_r, E_\theta, E_z)$ (and $E_\theta = 0$ is imposed later), and applied magnetic induction $\boldsymbol{B} = (0, 0, B_z)$. The shear stress components (e.g., $\tau_{rz}$) and the heat flux components (e.g., $q_z''$) are each expanded in the boundary-fitted coordinates, under the thin-layer approximation. The metric components (e.g., $\xi_r$) and the Jacobian of the $(r, z) \rightleftharpoons (\xi, \eta)$ transformation, $\sqrt{g} = (\xi_r \eta_z - \xi_z \eta_r)^{-1}$, are calculated using the specified grid. $\dot{q}_N$ is given by

$$\dot{q}_N = G_f \beta_f \bar{\sigma}_f n_0 \Phi \sim \rho \Phi \tag{2}$$

where $\beta_f$ is the atom-fraction of the fissionable isotope to atoms of background gas.

The Baldwin-Lomax algebraic turbulence model[14] is used to predict eddy viscosity and thermal conductivity coefficients. The effect of MHD interaction on turbulence modeling was beyond the scope of this work and is neglected. Rankin[15] reports that, in general, the degree of turbulence is reduced by the MHD interaction because some of the turbulence energy is dissipated as Joule heating, and that turbulence damping was not an important factor in the supersonic flows he studied due to the high mean velocities.

**Table 1 $UF_4$, He, and $UF_4$-(94%)He working fluid mixture properties[a]**

| Property | $UF_4$ | He | $UF_4$-He mixture |
|---|---|---|---|
| $M_w$, kg/kg-mole | 311.15 | 4.0 | 22.43 |
| $R$, J/kg·K | 26.72 | 2078.5 | 370.68 |
| $\gamma$ | 1.09 | 1.666 | 1.482 |
| $c_p$, J/kg·K | 323.61 | 5190.0 | 1139.4 |
| $\mu_l$, kg/m·s | $8.67 \times 10^{-5}$ | $7.55 \times 10^{-5}$ | $1.0 \times 10^{-4}$ |
| $k_l$, W/m·K | 0.031 | 0.589 | 0.4609 |
| $Pr$ | 0.901 | 0.665 | 0.247 |

[a]All properties tabulated at 2000 K.

A viable working fluid should contain a significant fraction of a fissionable isotope (e.g., $^{235}U$), to insure adequate fission densities, and should have an effective $\gamma$ high enough (e.g., $\gamma \geq 1.3$) for reasonable generator operation. Based on past work,[4,16] impetus existed to consider a $UF_4$ and helium working fluid mixture. A 6 (mole-%) $UF_4$, 94% He generator working fluid was selected for the study. Estimates of the high-temperature properties of the pure $UF_4$ and He constituents are presented in Table 1 along with the properties of the $UF_4$-He mixture, and are based on property data compiled from a number of sources.[17,18]

The flows analyzed in this work are supersonic throughout the generator, except immediately adjacent to the walls where the flow is subsonic as a consequence of no-slip. At the supersonic inflow boundary, $\bar{P}$ and $\bar{T}$, $M_R$, $S$, and inlet boundary-layer thickness (typically 1 mm) are specified. The inlet axial flow profile $[w(z)/u(z)]$ is calculated based on the inlet duct wall geometry and using a simple von Karman integral analysis to estimate the flow angle within the boundary layer in a best effort to eliminate "leading-edge" shocks due to flow angle mismatch at the inlet plane. Full extrapolation of the primitive variables ($\rho$, $\boldsymbol{u}$, and $\bar{e}$) is used at the supersonic outflow. At the walls the temperature is specified and no slip ($\boldsymbol{u} = 0$) and $\partial P/\partial n = 0$ (where $n$ is the direction normal to the wall) are imposed. A more detailed treatment of the boundary condition modeling is found in Ref. 5.

The governing equations in finite difference form are integrated using MacCormack's explicit predictor-corrector method.[19] The original method, without source terms, is second-order accurate in both space and time, and is suitable for integrating the time-dependent MHD fluid equations. Local time-stepping[20] is used to accelerate convergence into steady state. Where required for resolving shock waves and suppressing numerical oscillations, second-[21] and fourth-order[22] damping terms were introduced. The method has been found to be quite stable for integrating the MHD equations with their large body force and power source terms.[5]

### B. Electromagnetics

Under the modeling assumptions stated at the beginning of this section, the governing equations of electromagnetics may be written as $\nabla \cdot \boldsymbol{J} = 0$ and $\nabla \times \boldsymbol{E} = 0$, where $\boldsymbol{J}$ ($\simeq \boldsymbol{J}_e = -en_eU_e$) is related to $\boldsymbol{E}$ through the generalized Ohm's law relationship $\boldsymbol{J} + \mu_e \boldsymbol{J} \times \boldsymbol{B} = \sigma_e(\boldsymbol{u} \times \boldsymbol{B} + \boldsymbol{E})$, where consistent with the local models for $\sigma_e$ and $\mu_e$, discussed below, the electron pressure gradient induced electrical field is neglected. The notation $\boldsymbol{J} = (J_r, J_\theta, J_z)$, $\boldsymbol{E} = (E_r, E_\theta, E_z)$, $\boldsymbol{u} = (u, v, w)$, and $\boldsymbol{B} = (0, 0, B_z)$ is used in the development that follows. After Roseman,[8] $\varphi$ is defined such that $rJ_r = (\partial\varphi/\partial z)$ and $rJ_z = -(\partial\varphi/\partial r)$, which assures that current continuity is satisfied, given the tangential-symmetry imposed earlier. With tangential-symmetry, $\nabla \times \boldsymbol{E} = 0$ requires that $E_\theta(r) = E_\theta(r) = (\text{const}/r)$. At both the anode and the cathode, $E_\theta$ is necessarily zero—i.e., the electrodes are treated as perfect conductors ($\sigma_e \rightarrow \infty$). Therefore, it may be concluded that $E_\theta(r) = E_\theta(r) = 0$ within the MHD generator active volume. $\boldsymbol{E}$ is therefore expressed as $\boldsymbol{E} = (E_r, 0, E_z)$, where the radial $E_r$ and the axial $E_z$ components are related through $\nabla \times \boldsymbol{E} = 0$ by $(\partial E_r/\partial z) = (\partial E_z/\partial r)$. Using this relationship along with the generalized Ohms law gives the elliptic Poisson equation

$$\frac{\partial}{\partial r}\left(\frac{1}{\sigma_e}\frac{\partial\varphi}{\partial r}\right) + \frac{\partial}{\partial z}\left(\frac{1}{\sigma_\perp}\frac{\partial\varphi}{\partial z}\right) = \frac{\partial}{\partial z}\left[(\beta_e u + v)B_z\right] \quad (3)$$

where $\sigma_\perp \equiv \sigma_e/(1 + \beta_e^2)$ is the Hall electrical conductivity, and $\beta_e$ ($\equiv \mu_e B_z$) is the electron Hall parameter.

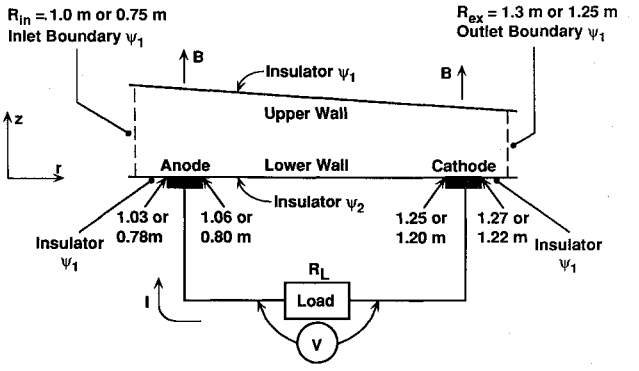


**Fig. 3 Schematic diagram of electromagnetics solver problem space—MHD generator with linearly decreasing duct height.**

Equation (3) is transformed into the same generalized curvilinear boundary-fitted coordinate system ($\xi$, $\eta$) employed with the fluid flow equations, and requires that the magnitude of the dependent variable $\varphi$ be specified on all boundaries as shown in Fig. 3. The inlet (upstream) and outlet (downstream) boundaries are artificial surfaces, taken to coincide with the inlet and outlet boundaries of the fluid problem. The inlet surface is set, therefore, at some arbitrary distance upstream of the anode; similarly, the outlet surface is placed at some arbitrary distance downstream of the cathode. The component of the conduction current density normal to these planes is required to be zero ($\boldsymbol{J} \cdot \boldsymbol{n} = 0$). The generator cross-sectional variation is determined by the top insulator duct wall. The flat bottom wall is composed of the anode and cathode rings and surrounding insulator surfaces. At the electrode surfaces $\boldsymbol{J} \cdot \boldsymbol{e}_\xi = 0$ is imposed where $\boldsymbol{e}_\xi$ is a unit vector tangent to the electrode surface. At insulator surfaces, $\boldsymbol{J} \cdot \boldsymbol{n} = 0$ is enforced. These boundary conditions are enforced by setting $\varphi = \varphi_1$ on all boundaries except the insulator surface between the electrodes on the lower wall at which $\varphi = \varphi_2$. The overall electrical solution is obtained by solving Eq. (3) using an alternating direction implicit (ADI) scheme. $\varphi_1$ and $\varphi_2$ are related to $I$ through an integral constraint at the electrodes [i.e., $I = \int_A \underline{J} \cdot \underline{n}\, dA = 2\pi(\varphi_1 - \varphi_2)$]. Subsequent load current values are obtained from $I_{new} = [(1 - \omega)I_{old} + (V_L/R_L)\omega]$, where $V_L$ is the voltage across the load ($= \int_L \boldsymbol{E} \cdot \boldsymbol{dl}$). Additional details on the electromagnetics solution are found in Ref. 5.

### C. Plasma Physics Modeling

The plasma transport property modeling is consistent with the continuum description of the MHD generator and is commensurate with other engineering MHD work.[7,23] The modeling was influenced by discussions with Appelbaum.[24] Deese and Hassan,[25] and more recently Watanabe et al.,[24] provide good summaries of work on fission fragment induced plasmas.

The plasma of concern in this work is a collision-dominated, weakly ionized plasma in which fission fragment induced ionization provides the dominant source of free electrons that affect electrical conductivity. The two-temperature model of Kerrebrock[26] is used in that the thermal electrons, responsible for the local plasma properties, are assumed to be in a Maxwell-Boltzmann distribution at $T_e$, which can be higher than the working fluid static temperature $T$. Steady-state number

density and energy balances in which spatial gradients are neglected are used to calculate $n_e$ and $T_e$, needed to determine the transport properties.

The dominant source of thermal electrons are the subexcitation energy electrons slowing down in a high-energy (non-Maxwellian) tail sustained by $S_{ff}$ (cf. Watanabe et al.[24]). $S_{ff}$ is assumed to be much larger than the electron source due to thermal ionization, and is given by $S_{ff} = \dot{q}_N/w_{ff}$, where $\dot{q}_N$ is the fission power density [Eq. (2)] and $w_{ff}$ is typically 20 eV $\leq w_{ff} \leq$ 50 eV; $w_{ff} = 35$ eV is used in the present study. Three-body electron-stabilized recombination is assumed to be the principle thermal electron loss mechanism at the pressures and temperatures of this study. The electron number density balance is therefore given by $\alpha_3 n_e^3 \simeq S_{ff}$ $(=\dot{q}_N/w_{ff})$, where $\alpha_3 = C_3 T_e^{-9/2}$ is the three-body recombination coefficient, and where $C_3 = 1.2 \times 10^{-20}$ (in S.I. units) is an estimate.[5] This same cube root dependence of $n_e$ on the nuclear reaction rate was used by Braun[27] to predict the number density of $^3He^+$ in the case of ionization during an expansion of $^4He$ gas, seeded with $^3He$, in a nozzle in the presence of a neutron flux where the $^3He$ seed, experiencing $(n, p)$ reactions, plays an analogous role to the fissionable isotope in this study. The electron number density balance can be rearranged to yield[5,6]

$$n_e = (S_{ff}/\alpha_3)^{1/3} = a_1 n_0^{1/3} \Phi^{1/3} T_e^{3/2} = a_1 (P/kT)^{1/3} \Phi^{1/3} T_e^{3/2} \quad (4)$$

which shows the functional dependence of $n_e$ on the fluid thermodynamic conditions ($P$ and $T$), $\Phi$, and $T_e$; $a_1$ $[=(G_f \bar{\sigma}_f \beta_f / w_{ff} C_3)^{1/3}]$ is a constant that depends on the working fluid physical data.

The thermal electron "fluid" gains energy by Joule heating, from the kinetic energy of the subexcitation electrons, and from three-body electron-stabilized recombination. The thermal electrons lose energy by inelastic collisions with the background gas (neutral and ionized heavy particles). The energy balance on the thermal electron fluid gives the following relation for the electron temperature:

$$T_e = T + T_{NON} = T + \frac{m_H}{3 m_e \delta \bar{\nu}_{eH} n_e} \left[ (w_r + w_{ke}) S_{ff} + \frac{\underline{J} \cdot \underline{J}}{\sigma_e} \right] \quad (5)$$

In the equation above, $w_r$ is the energy release per recombination event (approximately the first ionization potential $\varepsilon$), $w_{ke}$ is the average kinetic energy of subexcitation energy electrons ($\simeq 0.3\varepsilon$[28]), $\bar{\nu}_{eH}$ is directly proportional to $\bar{Q}_{eH}$, and $(\underline{J} \cdot \underline{J})/\sigma_e$ is the local Ohmic heating density. The electron temperature is therefore equal to the background (heavy) gas temperature plus a nonequilibrium enhancement $T_{NON}$.

The scalar electrical conductivity $\sigma_e$ $(=en_e\mu_e)$, and the electron mobility $\mu_e$ are calculated using standard relationships. The electron mobility scales as $\mu_e \sim (T/P) T_e^{-1/2}$, so that the nonequilibrium temperature enhanced scalar electrical conductivity scales as $\sigma_e \sim (T/P)^{2/3} \Phi^{1/3} T_e$ for the fissioning plasma. Reminiscent of fully ionized seeded plasmas, the fissioning plasma exhibits a power law behavior rather than the strong exponential dependence on the electron temperature exhibited by partially thermally ionized seeded plasmas. This suggests that the fissioning plasma generators should exhibit the stability of fully ionized seeded gas generators. The simple plasma models also suggest that the fission fragment induced electrical conductivity and the generator electric power density both increase with increasing total Mach number,[16] motivating our choice of highly supersonic inlet conditions. Figure 4 shows the strong dependence of the electrical conductivity on $\bar{Q}_{eH}$ and $\delta$. For this figure we have used conditions typical of the generator inlet. The magnetic field strength is 5 T, the local radial Mach number and the swirl factor are 2.0 and 1.0, respectively, and the total temperature and pressure of the fluid are 3000 K and 5.066 MPa (50 atm), respectively, and

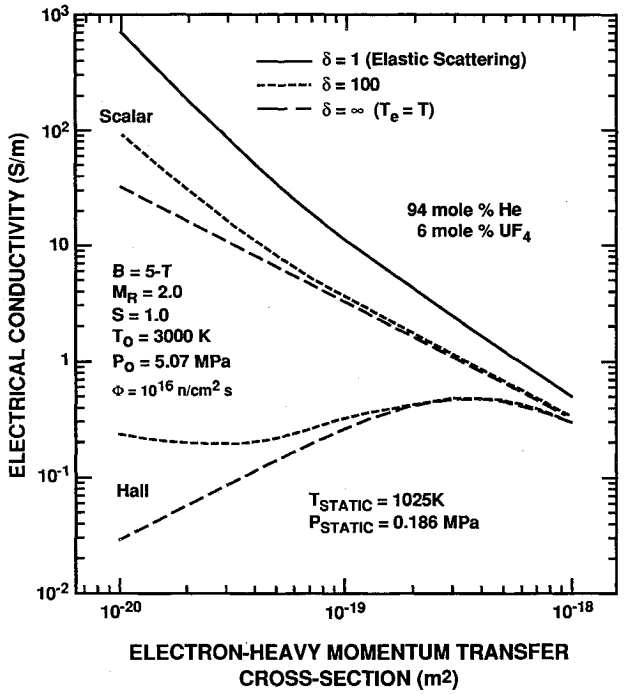


**Fig. 4 Scalar and Hall electrical conductivity of fissioning plasma as a function of $Q_{eH}$ and $\delta$.**

the neutron flux level is $1 \times 10^{16}$ n/cm$^2$·s. The fluid mixture is expected to have a momentum transfer cross section of nearly $1 \times 10^{-19}$ m$^2$, and an inelastic scatter factor between 100–1000[23]—i.e., $T_{NON} \to 0$—suggesting that the scalar electrical conductivity is $\mathcal{O}$ 1–10 S/m, and the Hall conductivity is $\mathcal{O}$ 0.1–1.0 S/m, with a corresponding electron mobility of $\mathcal{O}$ 0.1–1.0 T$^{-1}$.

### D. Overall MHD Solution

The overall two-dimensional MHD solution is obtained by iteration between a fluid solver and an electromagnetics solver, where each uses the same numerical grid. The structure of the numerical grid—the number of grid lines and the location of the grid lines—is dictated by the resolution requirements of the fluid solution. In this study a 101 × 101 grid is used. The grid spacing is uniform in the $\xi$ direction, and stretched in the $\eta$ direction so that at the walls the grid spacing has $\Delta z_{min} = 0.01$ mm and $\Delta z^+_{min} = 3$ (in law-of-the-wall coordinates), in order to assure that the turbulent boundary layer is well-resolved. An overall consistent MHD solution is obtained by a series of outer iterations between the fluid solver and the electromagnetics solver until the generator load current is converged upon.

## IV. Analysis

The effects of fission energy deposition and MHD interaction on important disk MHD generator flow variables are analyzed in this section. The effects of fissioning without MHD interaction ($B = 0$ T) are first described. The influence of fissioning and MHD interaction is then considered. Finally, two-dimensional predictions of the present study are compared with predictions of quasi-one-dimensional modeling.

### A. Effects of Fissioning Without MHD Interaction

A detailed study has been performed[5] on the effect of fissioning on the supersonic flowfield, in a variety of disk MHD generator duct geometries, in the absence of MHD effects (i.e., $B = 0$ T). The results clearly show the decelerating or diffusive effect of fission energy deposition; with increasing neutron flux levels, the velocity and stagnation pressure decrease while the stagnation temperature increases.

A few typical results are presented in Figs. 5 and 6 for a linearly decreasing duct height generator with the duct inlet located at $r = 1.0$ m, and an inlet duct height of 0.1 m. In these and subsequent calculations, the generator inlet conditions are $\tilde{T} = 3000$ K, $\tilde{P} = 5.066$ MPa (50 atm)—these dictated by the gas core reactor—$M_R = 2.0$ and $S = 1.0$ ($\Rightarrow$ total Mach number $= M_T \simeq 2.83$), the inlet boundary-layer thickness (at both the upper and lower walls) is assumed to be 1 mm, and the upper and lower wall temperatures are uniformly 2000 K. The radial profiles in Fig. 5 of the radial Mach number along the duct centerline (grid line 51 of 101) for flow with neutron flux levels of 0, $10^{16}$ n/cm$^2$·s, and $10^{17}$ n/cm$^2$·s show that the fission energy deposition in the fluid works to inhibit expansion (acceleration) of the duct flow as expected for Rayleigh flow.[29] Also noticeable in Fig. 5 are small inflections in the profiles due to the leading-edge oblique shocks generated by axial flow angle mismatch at the inlet boundary plane. Figure 6 shows the effect of neutron flux level on the static temperature and radial velocity component axial profiles at the lower wall at $r = 1.25$ m. The decelerating or diffusive effect of fissioning is again evident; however, note that at these high Mach numbers and corresponding low fluid densities, the diffusing influence of the fission energy deposition is small up to the very high neutron flux level of $1 \times 10^{16}$ n/cm$^2$·s.

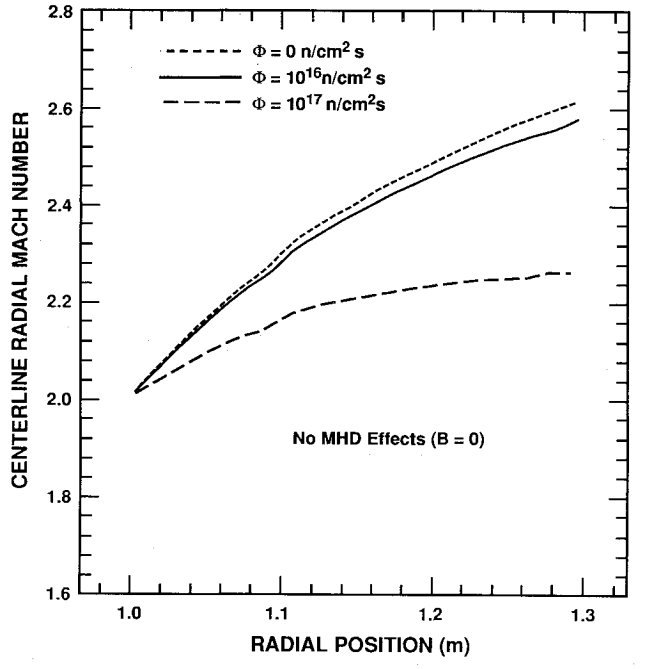


**Fig. 5 Centerline radial Mach number as a function of radial position and neutron flux level.**

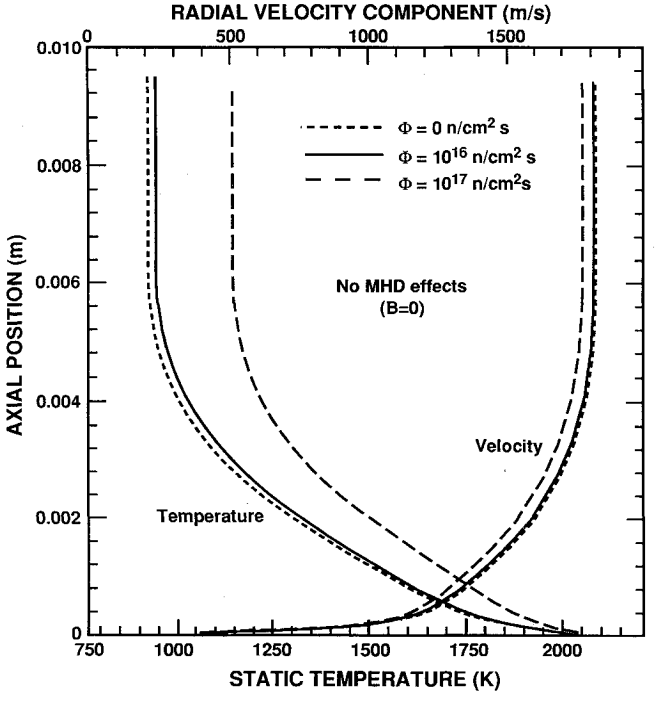


**Fig. 6 Radial velocity component and static temperature axial profiles at the lower wall at the cathode ($r = 1.21$ m).**

### B. Effects of MHD Interaction

This section examines MHD generator solutions that include spatially varying plasma physics properties obtained using the equilibrium electron temperature ($T_e \simeq T$) fissioning plasma model. The presented results are for the same generator inlet conditions specified above for the case without MHD effects. However, the neutron flux level is now fixed at $10^{16}$ n/cm$^2$·s, the generator inlet is located at 0.75 m (as compared to the 1.0-m duct inlet location used above), and the duct length is limited to 0.5 m (after which the neutron flux levels decrease rapidly). The electron number densities predicted by the simple plasma modeling are relatively low ($\mathcal{O}$ $10^{19}$/m$^3$), even at the very high neutron flux level of $10^{16}$ n/cm$^2$·s. In an attempt to insure MHD interaction sufficient to examine the important physical features of the flowfield, at the 5 T and 6 T magnetic induction levels considered, we have used $\tilde{Q}_{eH} = 5 \times 10^{-20}$ m$^2$, which is near that of helium, but is only half of what is the expected cross section. Considering Fig. 4, this means that we use a high scalar electrical conductivity (5–10 S/m) because of (an artificially) high electron mobility ($\mathcal{O}$ 1 T$^{-1}$), and also therefore a low Hall conductivity ($\mathcal{O}$ 0.1 S/m). As seen below, even with these optimistic plasma transport properties, the MHD interaction and electric power density levels are found to be low.

The radial profiles of the scalar electrical conductivity $[\sigma_e(r)]$ at the duct centerline (grid 51 of 101) and at the lower wall (grid 1 of 101), calculated as part of the overall MHD solution of the reference generator ($B = 5$ T, $R_L = 8$ Ω) problem, are provided in Fig. 7. Figure 8 shows the axial profiles $[\sigma_e(z)]$ of the scalar electrical conductivity at the center of the anode and at the center of the cathode for the reference generator.

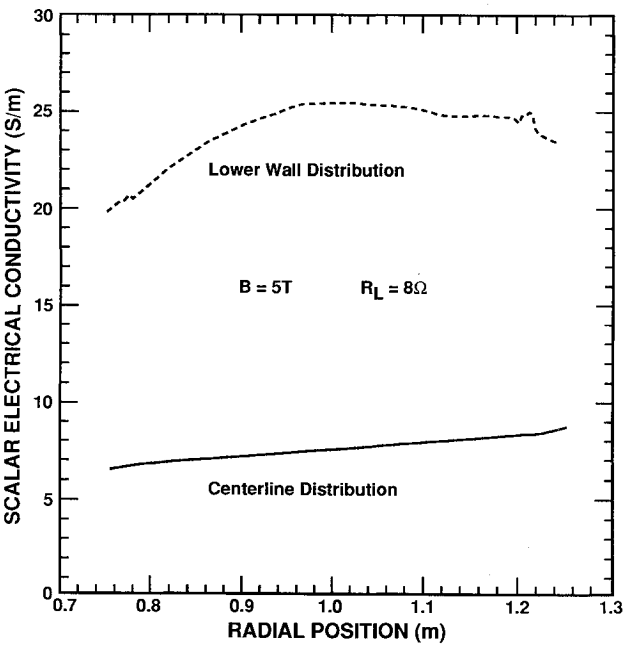


**Fig. 7 Centerline and lower wall radial profiles of scalar electrical conductivity in reference generator.**

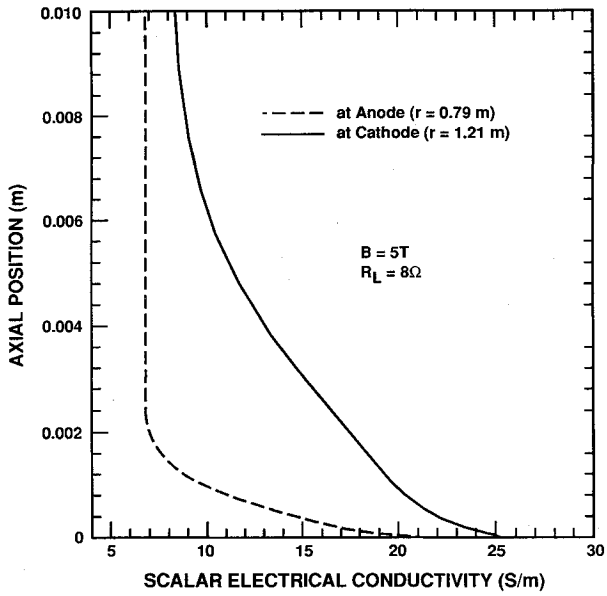


**Fig. 8 Scalar electrical conductivity at anode ($r$ = 0.79 m) and cathode ($r$ = 1.21 m) as a function of axial position in reference generator.**

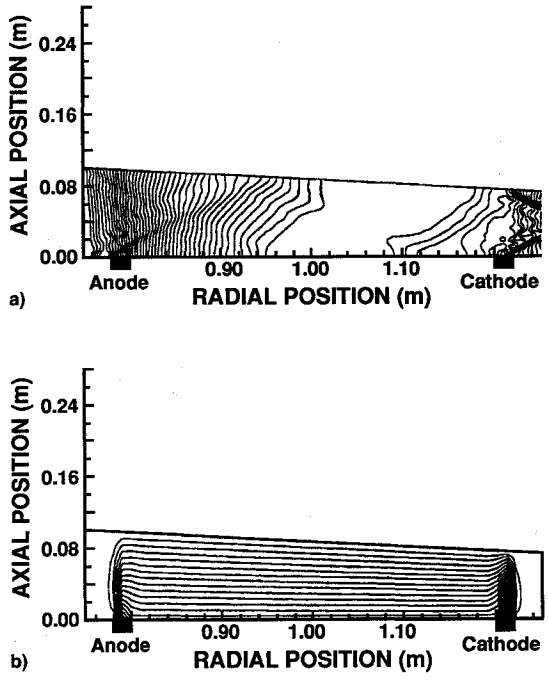


**Fig. 9 a) Static pressure and b) current density stream function contour plots of reference generator ($B$ = 5 T and $R_L$ = 8 Ω).**

The conductivity profiles are typical of the plasma property profiles obtained in the MHD generator solutions of this section. The $\sigma_e(r)$ lower wall distribution exhibits fluctuations (oscillations) in both the anode (0.78 m $\leq r \leq$ 0.8 m) and cathode (1.2 m $\leq r \leq$ 1.22 m) regions. These oscillations mirror radial fluctuations in the static pressure and temperature in the vicinity of both the anode and cathode due to locally high Ohmic heating rates resulting from current density nonuniformity at the electrodes (cf. Hurwitz et al.[30]). The load current leaves the anode through a small active ring (≤10% of the anode surface) at the upstream end of the anode, and enters the cathode through a small active ring at the downstream end of the cathode. Short-circuit current loops are driven over the remaining (inactive) portion of the electrode surface (see the current density stream function distribution in Fig. 9). The high local Ohmic heating rates at the active rings result in high local fluid temperatures and specific volume that result in locally increased electrical conductivity and cause weak oblique compression waves to be generated as the supersonic flow turns slightly to accommodate the local boundary-layer thickening. Apart from the near-electrode oscillations discussed above, the $\sigma_e$ radial profiles are fairly uniform throughout the duct.

Figures 10 and 11 provide comparisons of the stagnation temperature and pressure radial profiles along the duct centerline for generators with applied magnetic inductions of 0, 5, (reference case), and 6 T; the load resistance of each generator is 8 Ω that corresponds to an overall load parameter of $\zeta \simeq 0.5$. The combination of low MHD interaction levels and the short duct length (0.5 m), in which the high neutron flux level realistically can be maintained, results in extremely poor generator performance: The enthalpy extractions of the 5- and 6-T generators are 2.3 and 3.6%, respectively; the corresponding electric power densities are 140 and 190 $MW_e/m^3$;

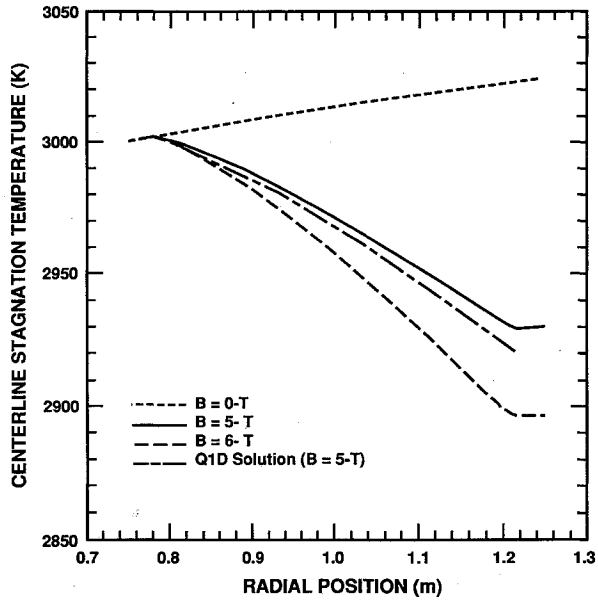


**Fig. 10 Centerline stagnation temperature as a function of radial position for $B$ = 0-, 5-, and 6-T generators.**

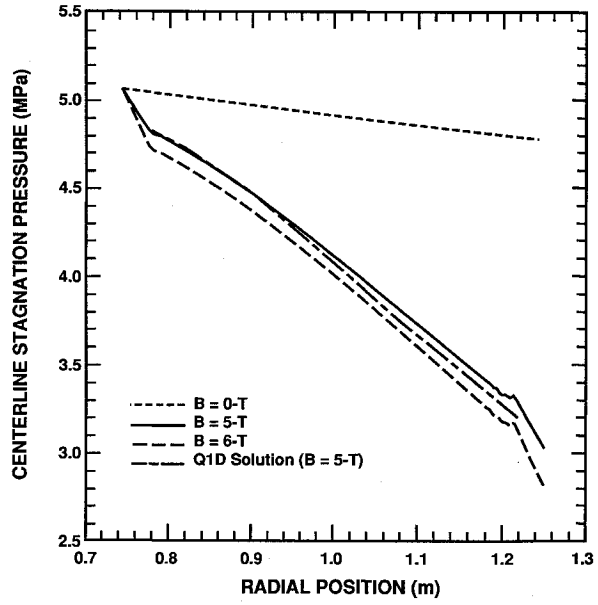


**Fig. 11 Centerline stagnation pressure as a function of radial position for $B$ = 0-, 5-, and 6-T generators.**

and the isentropic conversion efficiencies for the $B$ = 5- and 6-T generators are 14.9 and 20.4%, respectively. Figure 10 shows that outside (upstream or downstream) of the electrodes, no temperature change occurs; i.e., no enthalpy (or power) extraction occurs outside of the interelectrode region. In the case of no applied $B$-field, it is seen that the fission heating causes a linear increase in the total temperature. Figure 11 shows that the $B$ = 0-T generator exhibits a linear decrease in stagnation pressure due to the fission heat addition, and that for the $B$ = 5- and 6-T curves, a substantial total pressure loss occurs in the high interaction (open circuit) region just upstream of the anode and just downstream of the cathode. This suggests that the anode should be placed upstream (starting at $r$ = 0), and that the magnetic field should be designed to go to zero just downstream of the cathode so that the open circuit body force-induced total pressure losses are minimized.

The MHD interaction works to decelerate the flow as evident in Fig. 12 where the radial profiles of the radial Mach number along the center grid line of the $B$ = 0-, 5-, and 6-T generators are compared. At the fixed 8-Ω load resistance, the flow is increasingly decelerated—or inhibited from accelerating—as the applied magnetic induction, and therefore the MHD interaction, is increased. Both the radial and tangential body force components increase as the applied magnetic induction is increased. The predicted axial profiles of the radial velocity component at the cathode (at $r$ = 1.21 m) are compared in Fig. 13. Figure 13 also provides a comparison of the static temperature axial distributions in the boundary layer of the lower wall at the cathode ($r$ = 1.21 m). As the magnetic induction (and the MHD interaction) increases, the freestream flow is increasingly decelerated so that the freestream static temperature increases. A small temperature overshoot occurs very near the wall in all three profiles; the overshoot increases with increasing $B$-field primarily as a result of increased boundary-layer thicknesses at the higher magnetic induction levels.

A comparison of the axial profiles of the tangential velocity component at the cathode ($r$ = 1.21 m) for the $B$ = 0-, 5-, and 6-T generator cases is shown in Fig. 14. Because of the agreement in the magnitudes of the freestream tangential velocity component for the three curves, it is apparent that the $J_r B$ body force working against the flow in the freestream has little influence for the presented MHD interaction levels. However, the tangential velocity component has the potential

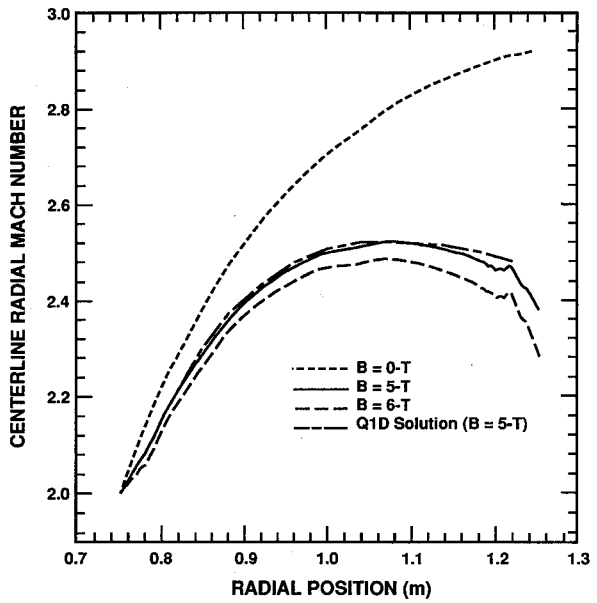


**Fig. 12 Centerline radial Mach number as a function of radial position for $B$ = 0-, 5-, and 6-T generators.**

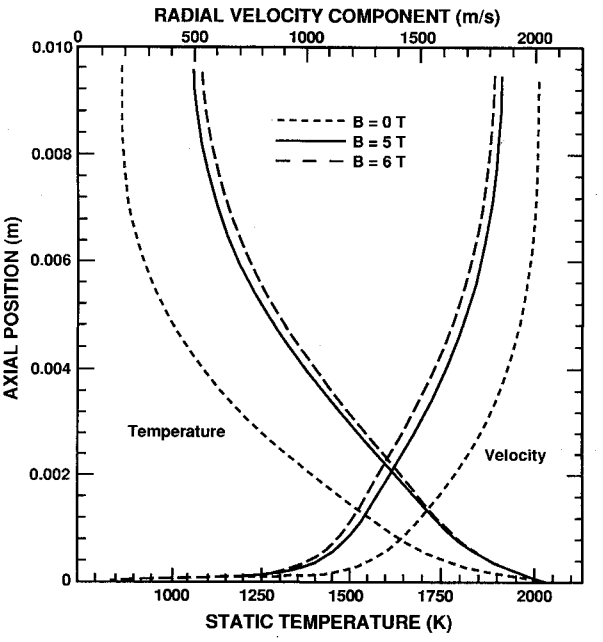


**Fig. 13 Radial velocity component and static temperature axial profiles at the lower wall at the cathode ($r$ = 1.21 m).**

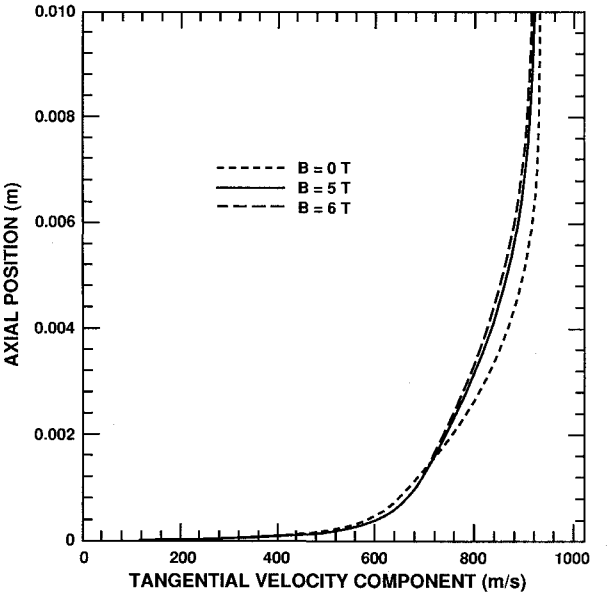


**Fig. 14 Tangential component of velocity as a function of axial position at cathode ($r$ = 1.21 m).**

for marked MHD effects. The ratio of the tangential components of the MHD body forces at the wall and the freestream can be estimated as[5] $(J_{r,w}/J_{r,\infty}) \simeq -(R_L/R_{\mathrm{MHD}})(\sigma_{\perp,w}/\sigma_{\perp,\infty})$. The magnitude of this ratio varies greatly with the load factor or load resistance and with wall temperature, and the body force component reverses direction from being oriented against the flow in freestream to being oriented with the flow near the wall. As seen in Fig. 14, even at these low MHD interaction levels, the tangential velocity component exhibits Hartmann flow characteristics in that as the $B$-field increases, the flow in the freestream is decelerated while the flow near the wall is accelerated.

Although not shown, the effects of varying $R_L$ on the MHD flow for a fixed $B$-field has also been investigated.[5,6] As expected, enthalpy extraction and the generator power density are greatest at the balanced load condition of $\zeta$ = 0.5 ($R_L \simeq$ 8 Ω). The $J_\theta B$ body forces, that work to decelerate the flow, increase as load resistance increases. Consequently, as the

load resistance increases, the stagnation pressure drop through the generator increases, the boundary layer tends to thicken, the temperature overshoot near the wall in the boundary region increases, and the radial velocity component decreases. With an increase in load resistance, the ratio of the $J_\theta B$ body force near the wall (with the flow) to the $J_\theta B$ body force in the freestream (against the flow) also increases. As a consequence, although the tangential velocity component in the freestream may experience only a very slight decrease, the tangential velocity component near the wall can undergo a significant increase; i.e., Hartmann flow effects lead to substantial changes in the tangential velocity profile as generator load resistance is varied from near short circuit to near open circuit.

### C. Comparisons with Quasi-One-Dimensional Flow Solver

A quasi-one-dimensional Euler solver with fission and MHD source terms was developed separate from and prior to this work.[4,16] Radial profile solutions for selected flow variables from the quasi-one-dimensional Euler solver have been compared with centerline radial profiles for the corresponding flow variables as predicted by the two-dimensional thin-layer Navier-Stokes solver developed in this work to indicate the relative influence of two-dimensional loss mechanisms.

Figure 10 includes a comparison of the quasi-one-dimensional stagnation temperature radial profile prediction with the center grid line stagnation temperature radial profile prediction from the two-dimensional solver. A greater enthalpy extraction level of the quasi-one-dimensional generator is evident in the larger temperature drop of the quasi-one-dimensional generator relative to that of the two-dimensional generator. Figure 11 includes a comparison of the quasi-one-dimensional stagnation pressure radial profile with the total pressure radial profile along the center grid line of the two-dimensional solver. The total pressure loss rate in the quasi-one-dimensional generator is greater than that of the two-dimensional generator, in spite of the frictional effects of the two-dimensional generator; however, the greater pressure drop of the quasi-one-dimensional solution simply corresponds to the higher enthalpy extraction. For the same enthalpy extraction, the less efficient two-dimensional generator would exhibit a larger pressure loss than the quasi-one-dimensional generator. Figure 12 shows good agreement between the quasi-one-dimensional and two-dimensional centerline radial Mach number radial profiles.

The quasi-one-dimensional and two-dimensional predictions of the reference MHD generator centerline flow variable profiles agree remarkably well. This suggests that two-dimensional loss mechanisms—including viscous effects (e.g., friction, heat transfer, boundary-layer defects, and negative current densities), wave structure (e.g., the oblique shock waves mentioned above), and the short circuit current loops at the electrode rings that are not resolved by the quasi-one-dimensional model—have a relatively small influence on the radial flow profiles at these low MHD interaction conditions. However, significant discrepancies between the two models occur in terms of global generator parameters such as total electric power (12% error) and isentropic efficiency (10% error).[5] It is significant to note however that while an overall two-dimensional MHD solution may require from $\frac{1}{2}$ to 1 cpu-day for convergence, the quasi-one-dimensional solver runs on the order of a cpu-second (on the same machine).

## V. Summary and Conclusions

A consistent methodology for solving the governing equations of steady-state, two-dimensional ($r$, $z$), viscous, supersonic, MHD flow of a fissioning, compressible, weakly ionized plasma in an outflow disk MHD generator is developed. The influence of fission energy deposition and MHD interaction on the behavior of important fluid mechanic, electromagnetic, and plasma physics variables are studied using the developed solution methodology. The results show that fissioning and MHD interaction both act to decelerate the flow. As expected, the MHD body forces increase with increasing applied $B$-field, at fixed generator load resistance and Hartmann flow effects are exhibited as the applied $B$-field is varied. The electric field is found to drive short-circuit current loops over the inactive portion of the anode and cathode. The result of the load current passing through the small (~10%) active surface area of the electrodes is locally high current densities leading to high Joule heating levels at the upstream edge of the anode and the downstream edge of the cathode. The enhancement in the Joule heating at the active electrode rings leads to weak oblique compression waves generated as the flow turns slightly to accommodate local boundary-layer thickening.

A comparison between the computed results from the two-dimensional MHD solver developed in this work and those from the quasi-one-dimensional MHD Euler solver shows that the two-dimensional effects have little influence on the radial profiles of the flowfield variables in these high Reynolds number, low MHD interaction level flows. The quasi-one-dimensional solver, however, overpredicts the generator enthalpy extraction and isentropic efficiency. The discrepancy between the two-dimensional Navier-Stokes and quasi-one-dimensional predictions of these global generator parameters is attributed to two-dimensional loss mechanisms, including boundary-layer velocity defect and nonuniform current density distribution effects at the finite-size electrodes.

The simple fissioning plasma transport property models suggest that the nonequilibrium temperature-enhanced scalar electrical conductivity of a fission fragment induced plasma is directly proportional to the electron temperature so that, reminiscent of a fully ionized plasma, the fissioning plasma should be quite stable. With the equilibrium electron temperatures expected in the $UF_4$-He working fluid, the electron number densities of the fission fragment induced plasma scale as the cube-root of the neutron flux level and are relatively low ($\mathcal{O}$ $10^{19}$ $m^{-3}$), even at very high neutron flux levels ($\mathcal{O}$ $10^{16}$ $n/cm^2 \cdot s$). The corresponding electrical conductivity levels and low MHD interaction levels, combined with the short duct length ($\leq$0.5 m) in which the high neutron flux levels realistically can be maintained, result in extremely low generator performance levels. This suggests that fission fragment induced ionization, by itself, is insufficient to effect the electrical conductivity levels needed for practical MHD power generation in the outflow disk MHD generator configuration considered.

## Acknowledgments

Portions of this work have been supported by the University of Florida, Gainesville, Florida, and the Air Force Wright Aeronautical Laboratories (AFWAL), Wright-Patterson AFB, Ohio. The AFWAL work was performed for the Innovative Science and Technology Directorate of the Strategic Defense Initiative within the Innovative Nuclear Space Power and Propulsion Institute (INSPI) at the University of Florida. Primary responsibility for the preparation of this article is credited to Edward T. Dugan. Discussions and guidance from Calvin C. Oliver at the University of Florida, on the fluid mechanics modeling and discussions with Jacob G. Appelbaum, during his tenure at INSPI, on the plasma physics modeling are gratefully acknowledged.

## References

[1]Dugan, E. T., Lear, W. E., Jr., and Welch, G. E., "Pulsed Gas Core Reactor for Burst Power," *Proceedings of the International Society of Optical and Engineering Symposium on Space Structures, Power, and Power Conditioning*, Vol. 871 (Los Angeles, CA), 1988, pp. 42–47.

[2]Maya, I., Anghaie, S., Diaz, N. J., and Dugan, E. T., "Ultrahigh

Temperature Vapor-Core Reactor—Magnetohydrodynamic System for Space Nuclear Electric Power," *Journal of Propulsion and Power*, Vol. 9, No. 1, 1993, pp. 98–104.

[3]Louis, J. F., "Disk Generator," *AIAA Journal*, Vol. 6, No. 9, 1968, pp. 1674–1678.

[4]Welch, G. E., Dugan, E. T., and Lear, W. E., Jr., "Disk MHD Generator for a Burst Power Gas Core Reactor," *Proceedings of the International Society for Optical Engineering Symposium on Space Structures, Power, and Power Conditioning*, Vol. 871 (Los Angeles, CA), 1988, pp. 15–24.

[5]Welch, G. E., "Analysis of the Magnetohydrodynamic Flow of a Fissioning Gas in a Disk MHD Generator," Ph.D. Dissertation, Univ. of Florida, Gainesville, FL, 1992.

[6]Welch, G. E., Dugan, E. T., and Lear, W. E., Jr., "Analysis of the MHD Flow of a Fissioning Gas in an Outflow Disk MHD Generator," AIAA Paper 93-3163, July 1993.

[7]Sutton, G. W., and Sherman, A., *Engineering Magnetohydrodynamics*, McGraw-Hill, New York, 1965.

[8]Roseman, D. F., "Current Distribution and Nonuniformity Effects in MHD Disk Generators," Ph.D. Dissertation, Stanford Univ., Stanford, CA; also Stanford HTGL Rept. 231, 1982.

[9]Rosa, R. J., "Hall and Ion-Slip Effects in a Nonuniform Gas," *Physics of Fluids*, Vol. 5, No. 9, 1962, pp. 1081–1090.

[10]Bird, R. B., Stewart, W. E., and Lightfoot, E. N., *Transport Phenomena*, Wiley, New York, 1960.

[11]Pullium, T. H., and Steger, J. L., "Implicit Finite-Difference Simulations of Three-Dimensional Compressible Flow," *AIAA Journal*, Vol. 18, No. 2, 1980, pp. 159–167.

[12]Vinokur, M., "Conservation Equations of Gas Dynamics in Curvilinear Coordinate Systems," *Journal of Computational Physics*, Vol. 14, No. 2, 1974, pp. 105–125.

[13]Thompson, J. F., Warsi, Z. U. A., and Mastin, C. W., *Numerical Grid Generation*, Elsevier, New York, 1985, Chap. III, pp. 95–133.

[14]Baldwin, B. S., and Lomax, H., "Thin Layer Approximation and Algebraic Model for Separated Turbulent Flows," AIAA Paper 78-257, Jan. 1978.

[15]Rankin, R. R., "Insulating Wall Boundary Layer in a Faraday MHD Generator," Ph.D. Dissertation, Stanford Univ., Stanford, CA; also Stanford HTGL Rept. 106, 1978.

[16]Welch, G. E., Dugan, E. T., Lear, W. E., Jr., and Appelbaum, J. G., "Modeling and Analysis of the Disk MHD Generator Component of a Gas Core Nuclear Reactor/MHD Rankine Cycle Space Power System," *Proceedings of the 25th Intersociety Energy Conversion Engineering Conference (IECEC)*, Vol. 2 (Reno, NV), 1990, pp. 449–454.

[17]Hassan, H. A., and Deese, J. E., "Thermodynamic Properties of $UF_6$ at High Temperature," NASA-CR-2373, Jan. 1974.

[18]Oliver, C. C., and Dugan, E. T., "Thermophysical Properties of $UF_6$-He Mixtures Relevant to Circulating Gas Core Reactor Systems," *Nuclear Technology*, Vol. 69, May 1985, pp. 161–169.

[19]MacCormack, R. W., "The Effect of Viscosity in Hypervelocity Impact Cratering," AIAA Paper 69-354, May 1969.

[20]Li, C. P., "Numerical Solution of Viscous Reacting Blunt Body Flow of a Multicomponent Mixture," AIAA Paper 73-202, Jan. 1973.

[21]MacCormack, R. W., and Lomax, H., "Numerical Solution of Compressible Viscous Flows," *Annual Review of Fluid Mechanics*, Vol. 11, 1978, pp. 289–316.

[22]Jameson, A., Schmidt, W., and Turkel, E., "Numerical Solutions of Euler Equations by Finite Volume Method Using Runge-Kutta Time Stepping Scheme," AIAA Paper 81-1259, June 1981.

[23]Rosa, R. J., *Magnetohydrodynamic Energy Conversion*, McGraw-Hill, New York, 1968.

[24]Watanabe, Y., Appelbaum, J., and Maya, I., "Electrical Conductivity of $UF_4$-K/KF Gas Partially Ionized by Fission Fragments," *Nuclear Science and Engineering*, Vol. 110, No. 2, 1992, pp. 109–127.

[25]Deese, J. E., and Hassan, H. A., "Analysis of Nuclear Induced Plasmas," *AIAA Journal*, Vol. 14, No. 11, 1976, pp. 1589–1597.

[26]Kerrebrock, J. L., "Magnetohydrodynamic Generators with Nonequilibrium Ionization," *AIAA Journal*, Vol. 3, No. 4, 1965, pp. 591–601.

[27]Braun, J., "Linear Constant-Mach-Number MHD Generator with Nuclear Ionization," *Plasma Physics (Journal of Nuclear Energy Part C)*, Vol. 7, Nov.–Dec., 1965, pp. 525–538.

[28]Rees, D. B., Leffert, C. B., and Rose, D. J., "Electron Density in Mixed Gas Plasmas Generated by Fission Fragments," *Journal of Applied Physics*, Vol. 40, No. 4, 1969, pp. 1884–1896.

[29]Shapiro, A. H., *Compressible Fluid Flow*, Vol. 1, Wiley, New York, 1954.

[30]Hurwitz, H., Jr., Kilb, R. W., and Sutton, G. W., "Influence of Tensor Conductivity on Current Distribution in an MHD Generator," *Journal of Applied Physics*, Vol. 32, No. 2, 1961, pp. 205–216.